Chinese Physics Letters

LETTER

Identifying and Tracking Magnetically Induced Polarization in $Fe_2Mo_3O_8$ by Static and Time-Resolved Second Harmonic Generation

Cite as: L. Y. Shi *et al*. 2026 *Chin. Phys. Lett.* **43** 090702

DOI CSTR

Recommended Articles

Second Harmonic Generation in Nanowires
Bi-Jun Zhao, Jian-Lin Zhao, and Xue-Tao Gan
Chin. Phys. Lett. **41**, 104201 (2024)

Second Harmonic-Induced Ultrafast Wrinkle Formation in Two-Dimensional Material
Xiaodong Wang, Yongzhao Zhang, Shuaishuai Sun, Jun Li, Shaobo Cheng, and Huaixin Yang
Chin. Phys. Lett. **42**, 047201 (2025)

Tracking Polarization Structure in $PtTe_2$ at Three-Dimensional Atomic Resolution
Aomiao Zhi *et al*.
Chin. Phys. Lett. **42**, 070717 (2025)

Giant Nonlinear Optical Response in Topological Semimetal Molybdenum Phosphide
Kai Hu, Yujie Qin, Liang Cheng, Youguo Shi, and Jingbo Qi
Chin. Phys. Lett. **40**, (2023)

Achieving Large Six Non-Volatile States via Monolayer Homologous Multiferroic $MoPtGe_2S_6$ in van der Waals Tunnel Junctions
Ruixia Yang, Xujin Zhang, Jianhua Xiao, Zhi Yan, Fang Wang, and Xiaohong Xu
Chin. Phys. Lett. **42**, 070705 (2025)

Nonvolatile Electrical Control of Transport Properties in Multiferroic $OsCl_2/Sc_2CO_2$ Heterostructure
Shi-Xu Wang, Shu-Xiang Qiao, Mei-Yan Ni, Xiao-Hong Zheng, Hua Hao, Hong-Yan Lu, and Ping Zhang
Chin. Phys. Lett. **42**, 080701 (2025)

A series journal of Chinese Physical Society distributed by IOP Publishing

Chinese Physics Letters

Chin. Phys. Lett. **43** 090702 (2026)

LETTER

DOI: 10.1088/0256-307X/43/9/090702
CSTR: 32039.14.0256-307X.43.9.090702

Identifying and Tracking Magnetically Induced Polarization in $Fe_2Mo_3O_8$ by Static and Time-Resolved Second Harmonic Generation

L. Y. Shi[1], D. Wu[2,3], T. Lin[1], S. J. Zhang[1,4], Q. M. Liu[1], Z. X. Wang[1], T. C. Hu[1], T. Dong[1,5], and N. L. Wang[5,2,1,*]

[1]International Center for Quantum Materials, School of Physics, Peking University, Beijing 100871, China
[2]Beijing Academy of Quantum Information Sciences, Beijing 100913, China
[3]Songshan Lake Materials Laboratory, Dongguan 523808, China
[4]Beijing National Laboratory for Condensed Matter Physics, Institute of Physics, Chinese Academy of Sciences, Beijing 100190, China
[5]Tsung-Dao Lee Institute, Shanghai JiaoTong University, Shanghai 201210, China

[*]Corresponding author. Email: nlwang@sjtu.edu.cn

Multiferroic materials offer a promising platform for ultrafast optical control of coupled magnetic and polar orders. However, a prerequisite for such control is to precisely identify how the magnetically induced polarization manifests itself on the ultrafast timescale, and then to probe its dynamics upon external perturbations. Here, we address this issue in the polar magnet $Fe_2Mo_3O_8$ by combining static and time-resolved second harmonic generation (SHG). Temperature-dependent static SHG reveals that, among the symmetry-allowed tensor elements, only $\chi_{ccc}^{(2)}$ exhibits a pronounced anomaly at the antiferromagnetic transition ($T_N \approx 60$ K), identifying $\chi_{ccc}^{(2)}$ as the nonlinear susceptibility tensor element coupled to the magnetically induced polarization. Guided by this result, time-resolved SHG selectively tracks the dynamics of this tensor element following ultrafast photoexcitation. We observe a rapid enhancement of the $\chi_{ccc}^{(2)}$-related SHG signal, followed by biexponential recovery. The response is independent of the pump polarization and reaches saturation at a remarkably low fluence, indicating a highly efficient coupling between optical excitation and the magnetically induced polarization. These results establish SHG as tensor-selective probe of ultrafast magnetoelectric dynamics and demonstrate the high sensitivity of the magnetically induced polarization in $Fe_2Mo_3O_8$ to optical excitation.

Multiferroic materials with coupled ferroelectricity and magnetism have attracted much attention due to their potential for mutual control of magnetization and polarization via electric and magnetic fields [1–3], and also provide a platform for ultrafast optical manipulation of different orders. Among optical techniques, time-resolved Kerr rotation and time-resolved second harmonic generation (SHG) are two important probes. Kerr rotation is widely used to study ferromagnetic materials [4–6], but its application to antiferromagnets (AFMs) is challenging due to the lack of net magnetization. In contrast, SHG is intrinsically sensitive to inversion symmetry breaking, making it a powerful tool for probing electric polarization and lattice structure. Moreover, the breaking of time-reversal symmetry in magnetically ordered systems can also contribute to the SHG response. As a result, SHG has been extensively employed to investigate noncentrosymmetric AFMs and multiferroics [7–13]. However, because the measured SHG signal generally contains contributions from multiple symmetry-allowed nonlinear susceptibility tensor elements, identifying the component associated with the magnetically induced polarization is essential for interpreting its ultrafast dynamics.

$Fe_2Mo_3O_8$ is a polar magnet that has attracted considerable interest [14–27]. Its structure, illustrated in Fig. 1(a), consists of alternating honeycomb Fe layers and Kagome Mo layers stacked along the c-axis. The lattice belongs to the space group $P6_3mc$, with a spontaneous polarization along the c-axis [28]. Below $T_N = 60$ K, the Fe spins exhibit antiferromagnetic order along the c-axis [29,30]. The magnetic ordering is accompanied by a structural distortion: oxygen atoms shift along the c-axis, giving rise to an additional polarization change ΔP and an increase of the Fe-O-Fe bond angle, which enhances the in-plane exchange coupling J [15]. These lattice modifications are attributed to exchange striction [15,16,31,32]. Subsequent studies have further uncovered a rich variety of magnetoelectric phenomena including topological magnon polarons and giant phonon magnetic moments [33,34]. In addition, a strong magneto-optical Kerr effect has been observed under circularly polarized pumping [21]. These characteristics make $Fe_2Mo_3O_8$ an ideal platform for identifying the nonlinear optical response associated with the magnetically induced polarization and tracking its ultrafast dynamics.

Here, we combine static and time-resolved SHG in a two-step approach. First, temperature-dependent static SHG measurements reveal a prominent reduction in only one of the second-order tensor elements, $\chi_{ccc}^{(2)}$, below the Néel temperature $T_N = 60$ K, identifying $\chi_{ccc}^{(2)}$ as the nonlinear susceptibility tensor element coupled to the magnetically induced polarization. Guided by this identification, we then use time-resolved SHG to track the ultrafast dynamics of this tensor element following photoexcitation. The $\chi_{ccc}^{(2)}$-related SHG signal exhibits an ultrafast enhancement within ~300 fs, followed by a biexponential recovery. The response reaches saturation at a remarkably low fluence of ~0.4 mJ/cm^2. This work demonstrates that combining static and time-resolved SHG provides a tensor-selective strategy for investigating ultrafast magnetoelectric dynamics in multiferroic materials.

The $Fe_2Mo_3O_8$ single crystal was grown by the chemical vapor transport method [35–37]. Static and time-resolved SHG measurements were performed on the natural ac-surface of the sample using a standard pump-probe system, with the experimental geometry illustrated in Fig. 1(b). The light source was a Ti:sapphire amplifier delivering 800 nm, 35 fs pulses at 1 kHz repetition. The pump beam was normally incident on the sample, while the probe beam was reflected from the sample at a small incident angle. The polarization of the incident probe was controlled by a half-wave plate, and the SHG signal was detected by a photomultiplier tube after filtering out the fundamental light. The pump spot size was ~120 μm and the probe spot size was ~90 μm. The fluence of the probe beam was ~0.2 mJ/cm^2.

Received 3 July 2026; accepted 3 August 2026; published 17 September 2026
© 2026 Chinese Physical Society and IOP Publishing Ltd. All rights, including for text and data mining, AI training, and similar technologies, are reserved.

Check for updates

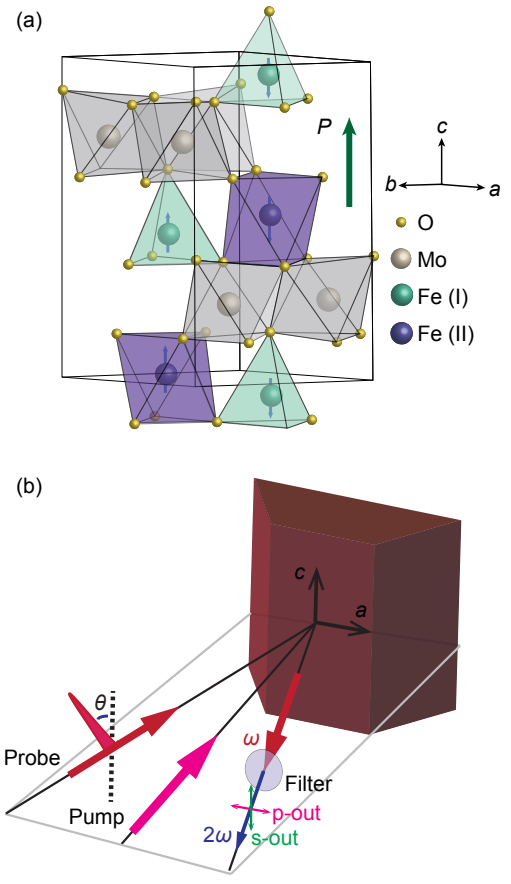

Fig. 1. (a) Crystal and magnetic structure of $Fe_2Mo_3O_8$. (b) Schematic illustration of measurement configuration of the TR-SHG.

For temperature-dependent measurements, the sample was mounted in a closed-cycle cryostat.

In magnetic materials, the second-order nonlinear polarization can be expressed as $P_i(2\omega) = \epsilon_0 \sum_{j,k}(\chi^{i(2)}_{ijk} + \chi^{c(2)}_{ijk})E_j(\omega)E_k(\omega)$, where $\chi^{i(2)}_{ijk}$ and $\chi^{c(2)}_{ijk}$ are the time-invariant and time-noninvariant nonlinear tensors, respectively [9,38]. For $Fe_2Mo_3O_8$ in the paramagnetic state (space group $P6_3mc$, point group $6mm$), the electric-dipole SHG tensor has only two independent nonzero components: $\chi^{(2)}_{ccc}$ and $\chi^{(2)}_{caa} = \chi^{(2)}_{aca}$, both of which are accessible in our ac-plane geometry. Below T_N, the magnetic point group becomes $\underline{6}m\underline{m}$, which allows nonzero c-type tensor components ($\chi^{c(2)}_{bbb} = -\chi^{c(2)}_{baa} = -\chi^{c(2)}_{aba} = -\chi^{c(2)}_{aab}$). However, for the present experimental geometry with near-normal incidence on the (001) surface, these magnetic-dipole tensor components do not contribute to the measured polarization configuration and are therefore not detected. We also checked an ab-cut sample and found no detectable signal at the magnetic transition, confirming that the magnetic-dipole contribution is negligible under our experimental conditions. Therefore, the measured SHG signal throughout this work is dominated by the electric-dipole contribution.

Figures 2(a) and 2(b) show the polar-angle-dependent SHG signals for s-out and p-out configurations at 20 K and 70 K. The SHG intensity can be expressed as $I_s \propto |\chi^{(2)}_{ccc}\cos^2\theta + \chi^{(2)}_{caa}\sin^2\theta|^2$ and $I_p \propto |2\chi^{(2)}_{aca}\sin 2\theta|^2$ [see the Supplemental Material (SM) for derivation]. The θ-dependent patterns are well reproduced by these expressions, as shown by the solid lines in Fig. 2. From the fitting to I_s, we find that $\chi^{(2)}_{ccc}$ and $\chi^{(2)}_{caa}$ have opposite signs, and $|\chi^{(2)}_{caa}| > |\chi^{(2)}_{ccc}|$. As the temperature decreases from 70 K to 20 K, a prominent reduction of I_s is observed only in the lobe near $\theta = 0°$ (where I_s is dominated by $\chi^{(2)}_{ccc}$), while the other lobe and all I_p lobes remain unchanged. The polarization-resolved measurements therefore establish $\chi^{(2)}_{ccc}$ as the nonlinear susceptibility tensor element associated with the magnetically induced polarization. This identification provides the basis for the time-resolved measurements presented below.

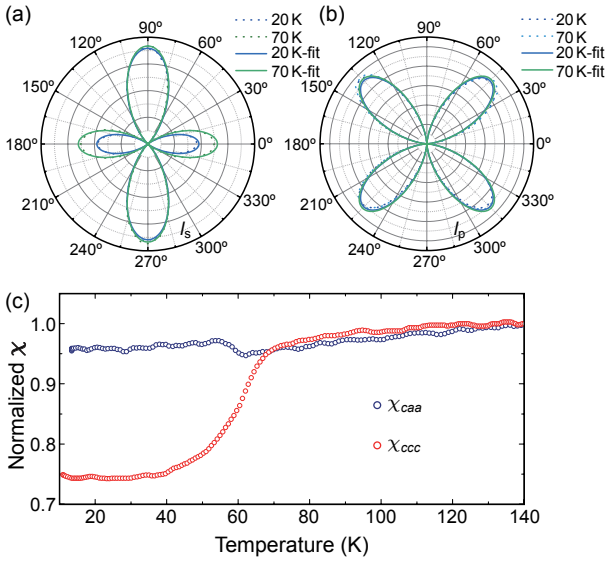

Fig. 2. (a) and (b) Polar plots of the SHG signal for s-out and p-out polarizations at 20 K and 70 K. The solid lines are fits to the expressions described in the text. (c) Temperature dependence of the SHG signals corresponding to $\chi^{(2)}_{ccc}$ and $\chi^{(2)}_{caa}$, normalized at 140 K. A clear anomaly is observed for $\chi^{(2)}_{ccc}$ near $T_N = 60$ K, while $\chi^{(2)}_{caa}$ shows no significant change.

We now turn to the temperature evolution of individual tensor elements. The SHG signal related to $\chi^{(2)}_{ccc}$ is obtained with s-in ($E^{\omega} \parallel c$) and s-out ($E^{2\omega} \parallel c$) polarization configuration. For comparison, $\chi^{(2)}_{caa}$ and $\chi^{(2)}_{aca}$ are measured using p-in/s-out and p-out at $\theta = 45°$, respectively. Figure 2(c) shows the temperature dependence of $\chi^{(2)}_{ccc}$. In the paramagnetic state, the SHG intensity decreases slightly upon cooling from 140 K, which is attributed to lattice anharmonicity. At T_N, a sharp drop of about 20% is observed in $\chi^{(2)}_{ccc}$, while $\chi^{(2)}_{caa}$ shows no significant change across the transition (apart from a barely visible kink that is negligible compared to the drop in $\chi^{(2)}_{ccc}$).

The electric-dipole SHG signal is generally considered to be proportional to the electric polarization. In $Fe_2Mo_3O_8$, a magnetically induced polarization modulation ΔP along the c-axis has been established at T_N [15,16]. The reduction of $\chi^{(2)}_{ccc}$ therefore indicates that the exchange-striction-induced polarization partially compensates the intrinsic polarization in the magnetically ordered state. Notably, only $\chi^{(2)}_{ccc}$ exhibits a pronounced change across the magnetic transition, while all other tensor components remain essentially unchanged. This selective response may be understood from the fact that the exchange-striction-induced ΔP is directed along the c-axis [15], and thus couples predominantly to the $\chi^{(2)}_{ccc}$ channel.

Since only $\chi^{(2)}_{ccc}$ is sensitive to the magnetic order induced polarization, the time-resolved SHG measurement is mainly focused on this tensor element using the s-in/s-out configuration. Figure 3(a) shows the time evolution of the pump-induced SHG change at 40 K under various pump fluences. The transient response contains two distinct features: a sharp decrease followed by a fast recovery ($\tau_1 < 1$ ps), and a subsequent slow rise to a plateau with a time constant τ_m that decreases from ~8 ps at low fluence to ~2 ps at saturation. The fast component is observed for all tensor elements, while the slow component is specific to $\chi^{(2)}_{ccc}$. To extract the time scales quantitatively, we fit the data using

$$\frac{\Delta I}{I} = \Theta(t)[a_1 \exp(-t/\tau_1) + a_m(1 - \exp(-t/\tau_m)) + c], \quad (1)$$

where $\Theta(t)$ is the Heaviside step function with a 35 fs rise time, a_1 and a_m are the amplitudes of the fast and slow components, respectively. The fitting curves are shown as solid lines in Fig. 3(a). The fluence dependence of the fitted time constant τ_m is presented in Fig. 4(a), while Fig. 4(b) shows the fluence dependence of the SHG

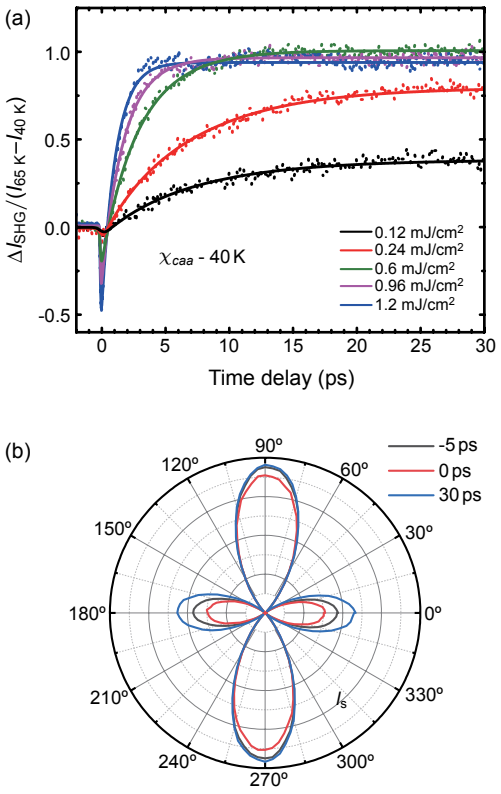

Fig. 3. (a) Transient dynamics of the SHG change (normalized to $I_{65\,K} - I_{40\,K}$) at various pump fluences. The solid lines are fits using Eq. (1). (b) Polarization dependence of the SHG signal in the s-out configuration at −5 ps (before pump), 0 ps (at the dip), and 30 ps, measured at 40 K with a pump fluence of 1.2 mJ/cm^2.

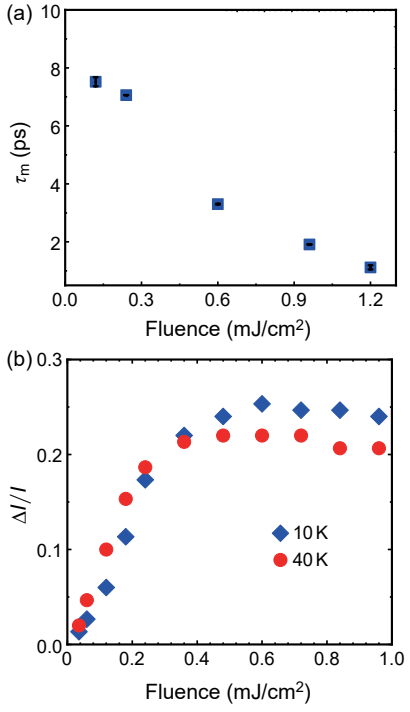

Fig. 4. (a) Fluence dependence of the time constant τ_m obtained from the fits in Fig. 3(a). (b) Fluence dependence of the relative SHG change ($\Delta I/I$) at 30 ps (on the plateau) at 10 K and 40 K.

signal change at 30 ps (on the plateau) at 10 K and 40 K.

We attribute the fast component ($\tau_1 < 1$ ps) to the ultrafast modulation of the spontaneous polarization by photo-excited carriers. The laser pulse excites electrons from the valence band to the conduction band, where delocalized carriers screen the dipole moments and temporarily reduce the SHG intensity. The polarization recovers as the carriers decay via electron-phonon scattering. This process is present in all tensor components, consistent with a transient modulation of the spontaneous polarization. This ultrafast polarization modulation process is an effective way to generate terahertz emission [39].

The slow component, in contrast, is specific to $\chi^{(2)}_{ccc}$, immediately suggesting that it originates from the magnetically induced polarization identified by the static SHG measurements. To confirm that the slow component is unique to the $\chi^{(2)}_{ccc}$ channel, we performed polar-angle scans of the s-out SHG signal at −5 ps (before pump), 0 ps (at the dip), and 30 ps (on the plateau), as shown in Fig. 3(b). At −5 ps, the pattern matches the static SHG. At 0 ps, all tensor components are uniformly reduced, consistent with the fast polarization screening. At 30 ps, only the $\chi^{(2)}_{ccc}$-related lobe is significantly enhanced, recovering toward the high-temperature (paramagnetic) pattern. This indicates that the slow component corresponds to the suppression of the exchange-striction-induced polarization associated with the loss of antiferromagnetic order. At saturation, the SHG signal fully recovers to the value measured above T_N, indicating the nearly complete suppression of the exchange-striction-induced polarization associated with the antiferromagnetic order. The saturation fluence is only ∼0.4 mJ/cm^2, representing a relatively low incident fluence compared with those typically used in previous optical studies of insulating multiferroics [40–42]. However, a quantitative comparison between different materials requires knowledge of the absorbed energy density, which depends on material-specific optical properties.

We also examined the polarization dependence of the pump pulse. The SHG response is independent of the pump polarization: circularly polarized, linearly polarized with different orientations, and 2 μm pumping (using an optical parametric amplifier) all produced essentially the same result (see SM). This contrasts with the circular-polarization-selective Kerr rotation reported previously in $Fe_2Mo_3O_8$ [21], where circularly polarized light was found to induce a net magnetization by selectively flipping spins in the antiferromagnetic sublattices. In our SHG measurements, which probe the lattice polarization rather than the magnetization directly, both circular and linear pumping efficiently suppress the exchange-striction-induced polarization. This suggests that the suppression of the exchange-striction-induced polarization associated with the antiferromagnetic order can be achieved by photoexcitation regardless of the pump polarization, whereas the generation of a net magnetization may require additional chiral selectivity.

Our time-resolved SHG measurements demonstrate that the magnetically induced polarization in $Fe_2Mo_3O_8$ can be efficiently suppressed by ultrafast optical pumping, with a fluence as low as ∼0.4 mJ/cm^2. However, the microscopic origin of this suppression cannot be uniquely determined from the present measurements. The absence of any detectable pump-polarization dependence is consistent with a thermally driven picture, in which the deposited energy, rather than the optical selection rule, dominates the transient response. The recovery of the magnetically induced polarization occurs on a timescale beyond 100 ps, indicating that the suppression of the exchange-striction-induced polarization is not followed by an equally fast recovery. Instead, the subsequent relaxation involves slower processes such as lattice thermalization and magnetic domain re-establishment. To achieve faster recovery and enable repetitive switching, alternative excitation pathways may be required. In particular, intense terahertz pulses, which can resonantly drive low-energy modes such as phonons or magnons, may offer a more direct and efficient route to manipulate the exchange-striction-induced polarization without significant lattice heating.

In summary, by combining static and time-resolved SHG measurements, we have investigated the ultrafast dynamics of the magnetically induced polarization in $Fe_2Mo_3O_8$. Static SHG reveals that only the $\chi^{(2)}_{ccc}$ tensor element exhibits a pronounced anomaly at T_N, identifying it as the nonlinear susceptibility component coupled to the

magnetically induced polarization. Guided by this identification, time-resolved SHG shows that this magnetically induced polarization can be efficiently suppressed within several hundred femtoseconds upon optical excitation, reaching saturation at a remarkably low fluence of ~0.4 mJ/cm^2, followed by a biexponential recovery. More broadly, this work demonstrates that combining static and time-resolved SHG provides a tensor-selective strategy for identifying and tracking magnetically induced polarization dynamics in multiferroic materials.

Acknowledgments

We would like to thank Profs. S. Dong, S. W. Cheong, J. Demsar for helpful discussions. This work was supported by the National Natural Science Foundation of China (Grant No. 12488201) and the National Key Research and Development Program of China (Grant No. 2024YFA1408701).

References

[1] Kimura T, Goto T, Shintani H, Ishizaka K, Arima T, and Tokura Y 2003 *Nature* **426** 55
[2] Tokura Y 2007 *J. Magn. Magn. Mater.* **310** 1145
[3] Fiebig M, Lottermoser T, Meier D, and Trassin M 2016 *Nat. Rev. Mater.* **1** 16046
[4] Beaurepaire E, Merle J C, Daunois A, and Bigot J Y 1996 *Phys. Rev. Lett.* **76** 4250
[5] Kise T, Ogasawara T, Ashida M, Tomioka Y, Tokura Y, and Kuwata-Gonokami M 2000 *Phys. Rev. Lett.* **85** 1986
[6] Ogasawara T, Ohgushi K, Tomioka Y, Takahashi K S, Okamoto H, Kawasaki M, and Tokura Y 2005 *Phys. Rev. Lett.* **94** 087202
[7] Fiebig M, Fröhlich D, Kohn K, Leute S, Lottermoser T, Pavlov V V, and Pisarev R V 2000 *Phys. Rev. Lett.* **84** 5620
[8] Nordlander J, De Luca G, Strkalj N, Fiebig M, and Trassin M 2018 *Appl. Sci.* **8** 570
[9] Matsubara M, Kaneko Y, He J P, Okamoto H, and Tokura Y 2009 *Phys. Rev. B* **79** 140411
[10] Sheu Y M, Ogawa N, Tokunaga Y, Chan H C, and Tokura Y 2018 *Phys. Rev. B* **98** 100301
[11] Cheong S W 2019 *npj Quantum Mater.* **4** 53
[12] Ron A, Zoghlin E, Balents L, Wilson S D, and Hsieh D 2019 *Nat. Commun.* **10** 1654
[13] Chu H, Roh C J, Island J O, Li C, Lee S, Chen J, Park J G, Young A F, Lee J S, and Hsieh D 2020 *Phys. Rev. Lett.* **124** 027601
[14] Le Page Y and Strobel P 1982 *Acta Crystallogr. B* **38** 1265
[15] Wang Y, Pascut G L, Gao B, Tyson T A, Haule K, Kiryukhin V, and Cheong S W 2015 *Sci. Rep.* **5** 12268
[16] Kurumaji T, Ishiwata S, and Tokura Y 2015 *Phys. Rev. X* **5** 031034
[17] Li Y, Gao G, and Yao K 2017 *EPL* **118** 37001
[18] Kurumaji T, Takahashi Y, Fujioka J, Masuda R, Shishikura H, Ishiwata S, and Tokura Y 2017 *Phys. Rev. B* **95** 020405
[19] Kurumaji T, Takahashi Y, Fujioka J, Masuda R, Shishikura H, Ishiwata S, and Tokura Y 2017 *Phys. Rev. Lett.* **119** 077206
[20] Yu S, Gao B, Kim J W, Cheong S W, Man M K L, Madéo J, Dani K M, and Talbayev D 2018 *Phys. Rev. Lett.* **120** 037601
[21] Sheu Y M, Chang Y M, Chang C P, Li Y H, Babu K R, Guo G Y, Kurumaji T, and Tokura Y 2019 *Phys. Rev. X* **9** 031038
[22] Wang W, Li P Z, Chang Y T, Liu M F, Lu C L, Lu X B, Zeng M, and Liu J M 2021 *Appl. Phys. Lett.* **118** 112901
[23] Csizi B, Reschke S, Strinić A, Prodan L, Tsurkan V, Kézsmárki I, and Deisenhofer J 2020 *Phys. Rev. B* **102** 174407
[24] Reschke S, Tsirlin A A, Khan N, Prodan L, Tsurkan V, Kézsmárki I, and Deisenhofer J 2020 *Phys. Rev. B* **102** 094307
[25] Stanislavchuk T N, Pascut G L, Litvinchuk A P, Liu Z, Choi S, Gutmann M J, Gao B, Haule K, Kiryukhin V, Cheong S W, and Sirenko A A 2020 *Phys. Rev. B* **102** 115139
[26] Wu F, Zhou J, Bao S, Li L, Wen J, Wan Y, and Zhang Q 2025 *Phys. Rev. Lett.* **134** 236701
[27] Bao S, Liao J, Huang Z, Shangguan Y, Ma Z, Zhang B, Cheng S, Xu H, Song Z, Dong S, Wu M, Kajimoto R, Nakamura M, Fennell T, Khalyavin D, and Wen J 2026 *Phys. Rev. Lett.* **136** 096502
[28] McCarroll W H, Katz L, and Ward R 1957 *J. Am. Chem. Soc.* **79** 5410
[29] Cotton F A 1964 *Inorg. Chem.* **3** 1217
[30] McAlister S and Strobel P 1983 *J. Magn. Magn. Mater.* **30** 340
[31] Chang Y, Weng Y, Xie Y, You B, Wang J, Li L, Liu J M, Dong S, and Lu C 2023 *Phys. Rev. Lett.* **131** 136701
[32] Chen Q, Miyake A, Kurumaji T, Matsuura K, Kagawa F, Miyahara S, Tokura Y, and Tokunaga M 2024 *Phys. Rev. B* **109** 094419
[33] Bao S, Gu Z L, Shangguan Y, Huang Z, Liao J, Zhao X, Zhang B, Dong Z Y, Wang W, Kajimoto R, Nakamura M, Fennell T, Yu S L, Li J X, and Wen J 2023 *Nat. Commun.* **14** 4359
[34] Wu F, Bao S, Zhou J, Wang Y, Sun J, Wen J, Wan Y, and Zhang Q 2023 *Nat. Phys.* **19** 1868
[35] Strobel P and Le Page Y 1983 *J. Cryst. Growth* **61** 329
[36] Strobel P, Le Page Y, and McAlister S 1982 *J. Solid State Chem.* **42** 242
[37] Satoh T, Van Aken B B, Duong N P, Lottermoser T, and Fiebig M 2007 *Phys. Rev. B* **75** 155406
[38] Fiebig M, Pavlov V V, and Pisarev R V 2005 *J. Opt. Soc. Am. B* **22** 96
[39] Shi L Y, Wu D, Wang Z X, Lin T, Zhang S J, Liu Q M, Hu T C, Dong T, and Wang N L 2020 *Acta Phys. Sin.* **69** 204206 (in Chinese)
[40] Johnson J A, Kubacka T, Hoffmann M C, Vicario C, de Jong S, Beaud P, Grübel S, Huang S W, Huber L, Windsor Y W, Bothschafter E M, Rettig L, Ramakrishnan M, Alberca A, Patthey L, Chuang Y D, Turner J J, Dakovski G L, Lee W S, Minitti M P, Schlotter W, Moore R G, Hauri C P, Koohpayeh S M, Scagnoli V, Ingold G, Johnson S L, and Staub U 2015 *Phys. Rev. B* **92** 184429
[41] Bowlan P, Trugman S A, Wang X, Dai Y M, Cheong S-W, Bauer E D, Taylor A J, Yarotski D A, and Prasankumar R P 2016 *Phys. Rev. B* **94** 184429
[42] Baldini E, Kubacka T, Mallett B P P, Ma C, Koohpayeh S M, Zhu Y, Bernhard C, Johnson S L, and Carbone F 2018 *Phys. Rev. B* **97** 125149